



Hendry, K., & Robinson, L.F. (2012). The relationship between silicon isotope fractionation in sponges and silicic acid concentration. Modern and core-top studies of biogenic opal. *Geochimica et Cosmochimica Acta*, 81, 1 - 12. <https://doi.org/10.1016/j.gca.2011.12.010>

Peer reviewed version

Link to published version (if available):
[10.1016/j.gca.2011.12.010](https://doi.org/10.1016/j.gca.2011.12.010)

[Link to publication record in Explore Bristol Research](#)
PDF-document

NOTICE: this is the author's version of a work that was accepted for publication in *Geochimica et Cosmochimica Acta*. Changes resulting from the publishing process, such as peer review, editing, corrections, structural formatting, and other quality control mechanisms may not be reflected in this document. Changes may have been made to this work since it was submitted for publication. A definitive version was subsequently published in *Geochimica et Cosmochimica Acta*, [VOL 81 (15 March 2012)] DOI: 10.1016/j.gca.2011.12.010

University of Bristol - Explore Bristol Research

General rights

This document is made available in accordance with publisher policies. Please cite only the published version using the reference above. Full terms of use are available:
<http://www.bristol.ac.uk/red/research-policy/pure/user-guides/ebr-terms/>

The relationship between silicon isotope fractionation in sponges and silicic acid concentration: modern and core-top studies of biogenic opal

Katharine R. Hendry^{1,2} & Laura F. Robinson^{1,3}

1 Department of Marine Chemistry and Geochemistry, Woods Hole Oceanographic Institution, Woods Hole, MA 02543, USA

2 School of Ocean and Earth Sciences, University of Cardiff, Main Building Park Place, CF10 3AT, UK

3 Department of Earth Sciences, University of Bristol, Wills Memorial Building, Queen's Road, BS8 1RJ, UK

ABSTRACT

Recent work has shown the silicon isotope composition, denoted by $\delta^{30}\text{Si}$, of deep-sea sponges reflects the concentration of ambient silicic acid ($\text{Si}(\text{OH})_4$) in seawater. However, existing calibrations are based predominantly on living sponges collected from the Southern Ocean. These data cannot, however, be used to determine whether other parameters that correlate with silicic acid in the Southern Ocean, such as temperature and salinity, influence $\delta^{30}\text{Si}$ of sponges. Furthermore, the published data do not demonstrate whether disaggregated core-top sedimentary spicules preserve the primary $\delta^{30}\text{Si}$ signal recorded in living sponges. Here, we address both of these issues. We refine and widen the existing calibration by including a global distribution of modern sponges. In addition, we provide the first systematic calibration from spicules picked from core-top sediments that covers sites from different ocean basins.

The relationship between Si(OH)_4 and $\delta^{30}\text{Si}$ in sponge spicules is the same in different ocean basins, between specimens that grew in different temperature and salinity conditions. Our core-top data agree well with the modern sponge calibration indicating there are no significant post-depositional effects or early diagenetic overprints. These two new datasets support the assertion that sponge $\delta^{30}\text{Si}$ can be used as a proxy for silicic acid concentrations in the past.

1. INTRODUCTION

The marine Si cycle is linked to global climate through coupling with the carbon cycle and the influence of tectonics and silicate weathering (West et al., 2005). In the modern ocean, biological precipitation of amorphous silica (opal) by diatoms is the dominant process that removes dissolved Si (silicic acid, or Si(OH)_4) from seawater, and is an efficient conveyor of organic carbon to the seafloor (Falkowski et al., 2004). The efficient uptake of Si by diatoms leads to a depletion of Si(OH)_4 in surface waters, such that in modern oceans diatom blooms are reliant on upwelling sources of Si(OH)_4 . The nutrient composition of upwelling waters, in particular the ratio of Si to other major nutrients, plays a strong role in the population structure of phytoplankton growing in surface waters (Sarmiento et al., 2004). Quantifying changes in the nutrient composition of deep and intermediate water is necessary in order to understand changes in surface production of biogenic opal, which provides a key control on atmospheric carbon dioxide (pCO_2) and global climate (Brzezinski et al., 2002; de la Rocha & Bickle, 2005; Hendry et al., 2010a, Ellwood et al., 2010).

The silicon isotope composition of biogenic opal ($\delta^{29}\text{Si}$ and $\delta^{30}\text{Si}$) has already been used to study modern Si cycling and past nutrient supply and utilization. Silicon is present in three stable isotopes: ^{28}Si (92.22%), ^{29}Si (4.68%) and ^{30}Si (3.08%). The permil Si isotopic composition is expressed relative to the NIST standard, NBS 28, according to Equation 1, where x is 29 or 30 (isotope ratios will be reported here as $\delta^{30}\text{Si}$):

$$\delta^x\text{Si} = \left\{ \frac{\left(\frac{{}^x\text{Si}}{{}^{28}\text{Si}} \right)_{\text{sample}}}{\left(\frac{{}^x\text{Si}}{{}^{28}\text{Si}} \right)_{\text{NBS28}}} - 1 \right\} \times 1000 \quad (1)$$

The $\delta^{30}\text{Si}$ of biogenic opal is influenced by a number of factors including seawater $\text{Si}(\text{OH})_4$ and biological fractionation. On timescales shorter than the residence time of Si in the ocean (estimated as between 9 and 15 thousand years; Tréguer et al., 1995; Georg et al., 2009), the isotopic composition of dissolved Si ($\delta^{30}\text{Si}(\text{OH})_4$) in the whole ocean is unlikely to change, although there are regional and vertical differences controlled by biological productivity and ocean circulation. The $\delta^{30}\text{Si}$ of diatom opal extracted from sediment cores have been used to reconstruct changes in ocean productivity, because of the Rayleigh-type fractionation processes that occur during uptake of $\text{Si}(\text{OH})_4$ in surface waters (de la Rocha et al., 1997, 1998). However, the interpretation of diatom $\delta^{30}\text{Si}$ is challenging because the lack of constraints on the spatial variation in $\delta^{30}\text{Si}(\text{OH})_4$, the composition of upwelling waters, mixing and export rates (e.g. Cardinal et al., 2007).

Sponges are benthic filter-feeding organisms that utilize dissolved Si for skeletal growth by precipitating opaline spicules of various morphologies. Recent work has shown that $\delta^{30}\text{Si}$ composition of deep-sea sponges from the Southern Ocean reflects the availability of dissolved Si during growth, and is therefore a potential proxy for past deep and intermediate water $\text{Si}(\text{OH})_4$ concentrations (Hendry et al, 2010a, 2011; Wille et al., 2010). There are no apparent species specific effects on Si fractionation, and tests on different types of spicules show that Si isotopes are homogeneous within an individual (Hendry et al., 2010a). Sponge spicules are ubiquitous in sediments throughout the oceans, but to date there has not been a thorough global calibration of the proxy that includes other ocean basins. The inclusion of other ocean basins in assessing the extent to which sponge spicules reflect $\text{Si}(\text{OH})_4$ is important because the $\text{Si}(\text{OH})_4$ concentration in Southern Ocean waters is strongly correlated with other environmental parameters such as temperature and salinity making it difficult to test the influence of a single parameter. There are some differences in temperature-salinity-Si regimes in the Southern Ocean, for example from coastal regions off the West Antarctic Peninsula (Hendry et al., 2010a), which indicate that $\text{Si}(\text{OH})_4$ concentration is indeed the major controller. However, the robustness of the $\text{Si}(\text{OH})_4$ - $\delta^{30}\text{Si}$ relationship needs to be tested further by investigating modern specimens from other oceanic basins and different water masses.

An important test of any paleoclimate proxy is whether core-top skeletal elements retain the signature of modern, living specimens despite post-depositional processes such as diagenesis, dissolution and averaging of vital effects over a number of individuals. These types of problems have been tested in, for example, Mg/Ca of

planktonic foraminifera, thought to be a measure of near surface temperatures (reviewed by Elderfield & Ganssen, 2000). Several studies have revealed several other factors that can control foraminiferal Mg/Ca during life, including growth rate, ontogeny, salinity, seasonality and vertical migration in the water column (e.g. Elderfield et al., 2002; Ferguson et al., 2008, Wit et al., 2010), and during post-depositional processes (e.g. Brown & Elderfield, 1996; Barker et al., 2003). As a result, individual specimens from core-top sediments exhibit large variability between and within individuals, and analyses show a reduction in variability as sample size increases (Anand et al., 2005).

In contrast to foraminiferal proxies, there has been no core-top calibration of sponge spicule $\delta^{30}\text{Si}$, although core-top spicules would provide a more appropriate comparison for downcore records and indicate any post-mortem, post-depositional, diagenetic or dissolution effects on sponge silicon isotopes. The high surface reactivity of biogenic opal (Dixit & van Capellan, 2002) makes it susceptible to rapid early diagenesis at the sediment-water interface. For example, the normalized aluminum content of opal $(\text{Al/Si})_{\text{opal}}$, increases over an order of magnitude between water column or sediment trap samples and surficial sediments (van Beusekom et al., 1997; Hendry et al., 2010b). A previous study has also found a potential diagenetic signal in diatom opal $\delta^{30}\text{Si}$, thought to be a result of surface dissolution effects, which may impact glacial-interglacial records by 10-30% (Demarest et al., 2009), although this is unlikely to have such an impact on spicules due to their more refractory nature (Maldonado et al., 2005).

Here, we extend the calibration for living specimens, and present new core-top spicule data, from the Atlantic and Pacific Oceans. We also use our data in combination with recently published experimentally derived assessments of silicon uptake rates (Maldonado et al., 2011) to explore the fractionation processes involved in biosilicification in sponges.

2. METHODS AND MATERIALS

2.1. Samples and sample preparation

Modern sponges were collected by trawl or dredge from the following localities (Table 1; Fig. 1), which have either co-located seawater samples or are located in well-constrained water masses:

- Scotia Sea and Drake Passage aboard the *R/V Nathaniel B. Palmer* in 2008 (full details in Hendry et al., 2010a);
- North Atlantic, from near Iceland, aboard the *Celtic Explorer* in 2008;
- North Pacific, from near Hawaii, *R/V Ka`Imikai-O-Kanalo*, in 2009. Further North Pacific samples were obtained from the Smithsonian collection (preserved in alcohol).

Specimens were also collected by hand by divers from the West Antarctic Peninsula and off Woods Hole, eastern Massachusetts (spring 2010).

The sponges were dried or frozen for transportation (with the exception of the samples from the Smithsonian). Organic matter was removed by heating three times in H₂O₂ (30% reagent grade) and then three times in concentrated in-house Teflon-

distilled HNO₃, followed by thorough rinsing in 18 MΩ Milli-Q water. Any remaining lithogenic particles were removed by hand, before a final clean in 50% in-house Teflon-distilled HNO₃/10% HCl, followed by five further Milli-Q water rinses. The spicules were dried, and 5-20mg of each sample was fused with high purity NaOH pellets (Fisher Scientific) at 730°C for 10 minutes in cleaned silver crucibles, quenched in Milli-Q water, sonicated and acidified according to Georg et al., 2006. These solutions can be stored for several months without change in δ³⁰Si.

Thirty to fifty core-top spicules were picked out of sediments from the Southern Ocean, the Argentine Shelf, the Iceland Basin, the Carolina Slope (North Atlantic, Keigwin, 2001) and Akademia Nauk Rise (Okhotsk Sea, North Pacific, Keigwin, 1998; Fig. 1, Table 1). The spicules were hand-picked from coarsely-sieved sediments, cleaned for clay contaminants by sonicating in ethanol (reagent grade), rinsed, heated in H₂O₂ (30% reagent grade) and then dried. The spicules were dissolved in 0.2 M NaOH solution at 100°C for three days, and then acidified, according to Hendry et al., 2010a. The solutions produced by this method cannot be stored on a long-term basis without a change in isotopic composition, but it does allow preparation and analysis of small samples of core top spicules (10 - 20μg Si) that cannot be prepared with the alkaline fusion method above as it would result in a solution of very low Si concentration. Spicules were picked from sediments dredged from two sites near Sars Seamount in the Drake Passage (*R/V Nathaniel B. Palmer*, cruises NBP0805 and NBP1103), prepared by alkaline fusion (Georg et al., 2006) and analyzed.

2.2. Analytical Procedures

2.2.1. Standard-sample bracketing without Mg doping

Silicon from the dissolved samples was quantitatively separated from metal contaminants using a cation exchange resin (Georg et al., 2006; Hendry et al., 2010a). The post-column samples were introduced into the Thermo Neptune Multi-Collector Inductively Coupled Plasma Mass Spectrometer (MC-ICP-MS) instrument at the Woods Hole Oceanographic Institution (WHOI) ICP-MS Facility.

Two methods were used to analyze Si isotopes: standard-sample bracketing and Mg doping. Mg doping was used because it has previously been reported as yielding higher precision and accuracy than standard-sample bracketing alone on the Neptune MC-ICP-MS (Cardinal et al., 2003). However, both methods yield accuracy and precision that are more than adequate for paleoceanographic applications.

Full operating conditions for the standard-sample bracketing method are described in Hendry et al., 2011. Mass bias and drift were accounted for by standard-sample bracketing, intensity matching samples and bracketing standards. Values of $\delta^{29}\text{Si}$ and $\delta^{30}\text{Si}$ were calculated offline using Equation 1, taking an average of the two bracketing standards for each sample, and repeat measurements were made for each sample (n=3). Data that did not meet strict quality control criteria were rejected, meeting guidelines described in Hendry et al., 2011. Repeat measurements (n = 14 runs) of sponge standard LMG08 show long-term reproducibility (using the mean of 3 standard-sample brackets per run) over 24 months of $\sim 0.06\text{‰}$ for $\delta^{29}\text{Si}$ and $\sim 0.15\text{‰}$ for $\delta^{30}\text{Si}$ ($2\sigma_{\text{SD}}$, Table 1; Hendry et al., 2010a, 2011). The relationship between $\delta^{29}\text{Si}$ and $\delta^{30}\text{Si}$ for all the modern sponge material analyzed by the method (slope = $0.515 \pm$

0.014, intercept = 0.009 ± 0.044 ; model II regression, 2σ confidence interval, $n = 17$) is consistent with mass dependent fractionation (Reynolds et al., 2007).

2.2.1. Standard-sample bracketing with Mg doping

Si and Mg isotopes were measured on the Neptune MC-ICP-MS in dual mode (peak-hopping) using a method adapted from Cardinal et al. (2003), such that ^{28}Si , ^{29}Si and ^{30}Si were measured in the first cycle and ^{24}Mg , ^{25}Mg and ^{26}Mg measured on the second cycle, with each cycle comprising 30 alternate measurements. Typical internal precision for the Si isotope ratios is comparable to the previous standard-sample bracketing method as described above (standard deviation $\sim 5 \times 10^{-6}$). The Si blanks of the Mg solution were the same as for 5% HCl and were less than 1% of the signal on the Si peak for each sample and standard. Blanks on ^{24}Mg are less than 5mV ($<0.05\%$ of the signal). Samples and bracketing standards were spiked with Mg standard (Inorganic Ventures), and intensity matched for ^{28}Si and ^{24}Mg signals within 10% (typically within 5%).

Si isotope ratios were corrected according to Cardinal et al. (2003). Our measurements of $^{25}\text{Mg}/^{24}\text{Mg}$ and $^{26}\text{Mg}/^{24}\text{Mg}$ show a consistent relationship for each run, with $\ln(^{25}\text{Mg}/^{24}\text{Mg})$ versus $\ln(^{26}\text{Mg}/^{24}\text{Mg})$ for repeat measurements of the sponge standard LMG08 showing a slope of 0.519 ± 0.006 (model II regression, 2σ confidence interval, $n = 13$) over a two month period (October to November 2010), which is in agreement with previous empirical estimates of fractionation (Galy et al., 2001; Cardinal et al., 2003) and consistent with the theoretical slope for either thermodynamic (0.521) or

kinetic (0.511) mass-dependent fractionation (Galy et al., 2001; Young et al., 2002). Within each run, $\ln(^{25}\text{Mg}/^{24}\text{Mg})$ values are linearly related to $\ln(^{29}\text{Si}/^{28}\text{Si})$. Repeat measurements ($n = 14$ runs) of standard LMG08 (using the mean of 3 standard-sample brackets per run) agree within error with previous measurements made using a range of methods (Hendry et al., 2011) and shows a reproducibility of $\pm 0.04\text{‰}$ for $\delta^{29}\text{Si}$ and $\pm 0.09\text{‰}$ for $\delta^{30}\text{Si}$ (2σ) over approximately 12 months, which is an improvement on conventional standard-sample bracketing (0.05‰ for $\delta^{29}\text{Si}$ and 0.15‰ for $\delta^{30}\text{Si}$, 2σ). Repeat measurements of sample aliquots, within and between runs, show typical variability $< \pm 0.1\text{‰}$ for $\delta^{29}\text{Si}$ and $\delta^{30}\text{Si}$.

3. RESULTS AND DISCUSSION

The aim of this study was to investigate the possible link between seawater $\text{Si}(\text{OH})_4$ concentrations and the isotopic composition of living sponges and core-top spicules by comparing data collected from specimens from other ocean basins to previously studied Southern Ocean samples. Here, we will discuss the modern and core-top spicule results, and present a biosilicification model that investigates the fractionation of isotopes by sponges during $\text{Si}(\text{OH})_4$ uptake.

3.1. *Sponge $\delta^{30}\text{Si}$ from living specimens*

The modern sponge $\delta^{29}\text{Si}$ values range from $+0.21\text{‰}$ to -2.99‰ and $\delta^{30}\text{Si}$ range from $+0.48\text{‰}$ to -5.72‰ (Fig. 2A, Table 1). The core-top values fall within a similar range of $\delta^{30}\text{Si}$ values, from -0.93‰ to -3.86‰ (Table 1).

Quantifying the fractionation of Si isotopes during the precipitation of biogenic opal requires values for the isotopic composition of both the opal and dissolved silicon in seawater in which the sponge grew ($\delta^{30}\text{Si}(\text{OH})_4$; Table 2). Si isotope fractionation by the sponges can be approximated to the difference between the isotopic composition of the seawater (Table 2) and the spicules assuming the opal is in equilibrium with the surrounding medium, which we will refer to as the “apparent isotope fractionation”:

$$\varepsilon_{\text{Si}} \approx \Delta\delta^{30}\text{Si} = \delta^{30}\text{Si}_{\text{opal}} - \delta^{30}\text{Si}_{\text{seawater}} \quad (2)$$

Deep-sea sponges live in a stable physical and chemical environment making it reasonable to assume that they show apparent isotopic fractionation in equilibrium with the surrounding medium. However, seawater $\delta^{30}\text{Si}(\text{OH})_4$ values are relatively poorly constrained due to limited datasets and natural variability, so a degree of uncertainty must be placed on calculated values of $\Delta\delta^{30}\text{Si}$ ($\sim 0.4\text{-}0.5\text{‰}$; see Fig. 2B).

$\Delta\delta^{30}\text{Si}$ in the low $\text{Si}(\text{OH})_4$ North Atlantic sponges ranged between approximately -1‰ and -2‰ . The sponge from the coastal region (very low $\text{Si}(\text{OH})_4$) near Woods Hole showed the heaviest isotopic compositions. The $\Delta\delta^{30}\text{Si}$ in $\text{Si}(\text{OH})_4$ -enriched North Pacific sponges was greater, ranging between approximately -5‰ and -6‰ , with one as isotopically light as -6.5‰ (Fig. 2B). This result is in agreement with previous findings that the apparent Si isotopic fractionation in sponges is related to ambient $\text{Si}(\text{OH})_4$ concentration (Fig. 2B; Hendry et al., 2010a; Wille et al., 2010; Hendry et al., 2011). A non-linear regression, fitting the dataset to a hyperbolic decay function, shows that the relationship between isotopic fractionation by sponges and ambient $\text{Si}(\text{OH})_4$ is statistically significant ($R^2=0.85$ for $\delta^{30}\text{Si}$ and $R^2=0.83$ for $\Delta\delta^{30}\text{Si}$; $n = 62$).

It is difficult to determine what factors control Si isotope fractionation in sponges from the Southern Ocean because there is such a strong correlation between environmental parameters such as Si(OH)_4 concentration, temperature and salinity. However, we can use the new data from other ocean basins and water masses with different temperature and salinity properties to deconvolve the influence of different environmental parameters and $\delta^{30}\text{Si}$. In contrast to the Southern Ocean plot, the plot of sponge $\Delta\delta^{30}\text{Si}$ versus temperature for samples from the North Atlantic and North Pacific shows that there is, in fact, no apparent influence of temperature (Fig. 3). Silicification in sponges is controlled by enzymatic processes, which would suggest that temperature could play an important role in Si uptake rates. However, experiments with live sponges show that increasing temperature does not influence Si uptake rates, consistent with our findings if Si uptake rate is the primary control over Si isotope fractionation (Frølich & Barthel, 1997). In addition to temperature, the data also show that there is no likely control on fractionation by salinity. The sponges grown in the North Pacific, for example, under similar Si(OH)_4 conditions have similar $\Delta\delta^{30}\text{Si}$ to those grown in the Southern Ocean despite having grown in significantly fresher waters (34.25-34.5 vs. ~ 34.7 in the Southern Ocean, all data from www.ewoce.org).

One important consideration of the results and interpretation of our data set in terms of major controls on silicification is that the sponge $\delta^{30}\text{Si}$ dataset presented here is dominated by samples from the deep-ocean (with the exception of two surface water sponges) and so not cover the entire range of environmental conditions of sponge

habitats. Further studies of shallow-living sponges, and particularly specimens from tropical shallow seas, would be helpful in extending our understanding of the differences and similarities of biosilicification in different habitats. However, our study does show that for the sub-thermocline conditions relevant to paleoceanographic applications based on spicules extracted from deep-sea sediment cores, the ambient Si(OH)_4 concentration is the dominant control over spicule $\delta^{30}\text{Si}$, supporting the use of sponge $\delta^{30}\text{Si}$ as a robust paleosilicic acid proxy.

3.2. Silicon fractionation model

Silicon uptake kinetics in sponges have been investigated through culture experiments on living specimens grown in media of differing Si(OH)_4 concentrations. Two different experimental set-ups have been used: initially based on explants, or pieces of sponges that have regenerated (Reincke & Barthel, 1997), and more recently on whole sponge specimens (Maldonado et al., 2011). In both cases, dissolved silicon was added to the growth medium in varying amounts, in the form of either Na_2SiF_6 , which can result in fluoride poisoning at high Si concentrations ($>200 \mu\text{M Si}$), or $\text{Na}_2\text{SiO}_3 \cdot 5\text{H}_2\text{O}$. The Si(OH)_4 concentrations in the growth medium are measured periodically to determine the Si uptake rate and at the end of the experiments the volume, wet and dry weights of the sponges are determined. Despite the differences in experimental set-up, both experiments show a non-linear relationship between silicon uptake and silicic acid concentration, resembling a Michaelis-Menton function (Reincke & Barthel, 1997; Maldonado et al., 2011).

The nature of the relationship between Si(OH)_4 concentration and uptake rate in sponges resembles that between Si(OH)_4 and Si isotopic fractionation. This non-linear relationship between $\Delta\delta^{30}\text{Si}$ and Si(OH)_4 is likely a result of fractionation during Si uptake, whereby as Si uptake rates increase with concentration, fractionation involved with these uptake processes also becomes enhanced (Wille et al., 2010). Although there are likely to be additional factors, this effect can be modeled assuming that the fractionation occurs in several steps: firstly as the Si is transported into the cell, secondly as the Si is polymerized, and thirdly as Si is lost from the cell (Fig. 4A).

Here, we build on the method developed by Wille et al. (2010), integrating i) our new data from different ocean basins, which shows that the fractionation processes appear to be universal in sponges grown in markedly different environments , and ii) the recent experimental Si uptake data from Maldonado et al. (2011).

The fractionation process can be expressed mathematically following Milligan et al., 2004 (Equation 3):

$$\Delta\delta^{30}\text{Si} \approx \varepsilon_f = \varepsilon_{it} + (\varepsilon_p - \varepsilon_{te}) \frac{v_E}{v_I} \quad (3)$$

Where ε_f = the total Si isotopic fractionation factor, ε_{it} = Si isotopic fractionation associated with transport into the cell, ε_p = Si isotopic fractionation associated with polymerization and ε_{te} = Si isotopic fractionation associated with transport out of the cell; v_E = rate of Si efflux and v_I = rate of Si influx (Fig. 4A). This equation has been rearranged by Wille et al. (2010) to form Equations 4 and 5:

$$\varepsilon_f = \varepsilon_{II} + \Delta\varepsilon_p \left\{ 1 - \frac{\frac{v_{\max p}}{\left(\frac{K_{mp}}{[Si(OH)_4]} + 1\right)}}{\frac{v_{\max I}}{\left(\frac{K_{mI}}{[Si(OH)_4]} + 1\right)}} \right\} \quad (4)$$

$$K_{mI} = v_{\max I} \times \frac{K_{mp}}{v_{\max p}} \quad (5)$$

where $\Delta\varepsilon_p = (\varepsilon_p - \varepsilon_{tE})$; K_{mI} and K_{mp} are the half saturation constants for incorporation and polymerization respectively, and $v_{\max I}$ and $v_{\max p}$ are the maximum incorporation and polymerization rates respectively. K_m is defined as the concentration at which the reaction rate is half of its maximum value (v_{\max}). In this case a low value of K_m represents a high affinity for $Si(OH)_4$.

K_{mp} and $v_{\max p}$ are poorly constrained, and highly variable even within a species (e.g. Maldonado et al., 2011). The two uptake experiments to date yielded K_{mp} and $v_{\max p}$ values of 46 μM and 19 $\mu mol\ h^{-1}\ g^{-1}$ (*Halichondria panicea*; Reincke & Barthel, 1997), and 74 μM and 1.7 $\mu mol\ h^{-1}\ g^{-1}$ (ranging from 0.03 to 5.2 $\mu mol\ h^{-1}\ g^{-1}$ for dry weights) respectively (*Axinella* spp; Maldonado et al., 2011). For every $v_{\max I}$ there is a unique value of $\Delta\varepsilon_p$ that corresponds to the minimum of the misfit function for a given dataset (Equation 6).

$$f(\varepsilon_{II}, \Delta\varepsilon, v_{\max I}) = \sum_{[Si(OH)_4]} (\varepsilon_{f,obs}([Si(OH)_4]) - \varepsilon_{f,pred}([Si(OH)_4]))^2 \quad (6)$$

Wille et al. (2010) found that, using the values for K_m and $v_{\max p}$ from Reincke & Barthel (1997), varying $v_{\max I}$ has little impact on the value of $\Delta\varepsilon_p$ at which the misfit function is at a minimum for values greater than $\sim 40\ \mu mol\ h^{-1}\ g^{-1}$ so in this model we used a fixed

323 $v_{\max l}$ of 120 $\mu\text{mol h}^{-1} \text{g}^{-1}$. We varied the remaining constants (ε_{tl} and $\Delta\varepsilon_{\text{p}}$) to predict
 324 $\Delta\delta^{30}\text{Si}$ using Equations 4 and 5, and optimized by finding the minimum of the misfit
 325 between predicted and measured $\Delta\delta^{30}\text{Si}$ (Equation 7):

$$326 \quad f(\varepsilon_{\text{tl}}, \Delta\varepsilon) = \sum_{[\text{Si}(\text{OH})_4]} (\varepsilon_{f, \text{obs}}([\text{Si}(\text{OH})_4]) - \varepsilon_{f, \text{pred}}([\text{Si}(\text{OH})_4]))^2 \quad (7)$$

327 Using only the values of K_{mp} and $v_{\max p}$ from Reincke & Barthel (1997) yields $\varepsilon_{\text{tl}} = -$
 328 1.55‰ and $\Delta\varepsilon_{\text{p}} = -5.3‰$ for the whole dataset, and $\varepsilon_{\text{tl}} = -1.46$ and $\Delta\varepsilon_{\text{p}} = -5.4‰$ for the
 329 Southern Ocean sponges considered alone (Fig. 4B). These are both slightly greater
 330 influx fractionations than that found by Wille et al. (2010) of -1.34‰, but all three
 331 values are within the uncertainties associated with the data.

332 Substituting the values of $v_{\max p}$ and K_{mp} that Maldonado et al. (2011) determined
 333 yields minimum misfit values of ε_{tl} and $\Delta\varepsilon_{\text{p}}$ of -1.74‰ and -5.11‰ for all modern
 334 sponges, a level of influx fractionation that is greater than the uncertainty in the data
 335 (Fig. 4C). The differences between the two datasets could have arisen due to bias in
 336 the two contrasting experimental set-ups, for example as a result of the physiological
 337 differences between explants, which show rapid regenerative growth, and whole
 338 specimens, or due to adverse effects of the dissolved silicon added to the medium
 339 (Maldonado et al., 2011). However, perhaps more importantly, the two studies focus
 340 on two different types of sponge. *H. panacea* is a seasonal sponge, silicifying rapidly in
 341 the spring for only a couple of months. In contrast, *Axinella* spp. is a slow growing,
 342 long-lived sponge that can live for decades (Maldonado et al., 2011). Such differences
 343 in growth behavior highlights that care must be taken when extrapolating the uptake
 344 kinetics of shallow-water sponges to our predominantly deep-water sponge dataset.

Nonetheless, this model is a useful first approach for understanding and quantifying Si isotope fractionation in sponges.

The fractionation constants calculated above were used to predict the sponge $\Delta\delta^{30}\text{Si}$ for each location in the dataset using Equations 4 and 5. As predicted from the prior misfit analysis, the observed and predicted $\Delta\delta^{30}\text{Si}$ values show a significant positive correlation ($r^2 = 0.82$ for both sets of uptake kinetics parameters) and the majority fall within error of a 1:1 line (Fig. 5). The exceptions are the sponges grown in very high Si(OH)_4 waters of the North Pacific ($>120\text{-}130\text{ }\mu\text{M}$). At such extreme Si availability, it could be that the relationship between net uptake, polymerization and ambient Si(OH)_4 weakens. Under very high Si(OH)_4 availability, hypersilicification can occur and is known to happen at Si(OH)_4 concentrations greater than $100\text{ }\mu\text{M}$, which could alter the apparent Si isotope fractionation (Maldonado et al., 1999). There is further evidence for a fundamental change in the fractionation mechanism at very high Si(OH)_4 from the core-top sample from Okhotsk Sea ($\text{Si(OH)}_4 \sim 200\text{ }\mu\text{M}$). However, the hypersilicification studies were carried out in shallow-living sponges from the Mediterranean and it is not yet known whether the same processes would occur in deep-sea sponges. Another possibility is that there are variations in deep water $\delta^{30}\text{Si(OH)}_4$ that are not captured by the values used in the model (Table 2). Further work is required to constrain the behavior of Si isotopes in both seawater and biogenic opal at extreme Si(OH)_4 concentrations.

It should be noted that the model used in our discussion is a simplification of sponge silicification. For example, the smaller microscleres may silicify in a different manner

to the large megascleres, which may complete formation external to the silicifying cell (reviewed by Müller et al., 2007), and there is evidence for different silicification mechanisms in demosponges compared to hexactinellids (Maldonado & Riesgom 2007). Understanding silicification mechanisms, and how they differ between individuals and clades, will be an important component in understanding Si isotope fractionation in sponges.

3.2.1. A comparison of sponges and diatoms

Above we have discussed the evidence for and possible mechanism behind variable fractionation factors in deep-sea sponges. By contrast, culture experiments have been used as evidence for a constant fractionation factor during Si uptake by diatoms, independent of temperature and species (de la Rocha et al., 1997). However, given that there is a relationship between silicic acid and growth rate in diatoms (e.g. Paasche, 1973; Nelson et al., 2001), and assuming fractionation processes occur during Si influx, polymerization and efflux, one might expect a link between Si isotope fractionation and ambient Si(OH)_4 concentration. One possible test of this fractionation is to investigate diatom Si uptake in natural settings. However, although reasonable for deep-sea sponges, the assumption of apparent equilibrium fractionation may not be necessarily be valid for diatoms because they can deplete ambient Si(OH)_4 during growth, and because surface waters are susceptible to processes such as upwelling, and advection or mixing of water masses.

In an attempt to account for this potential bias, we have collated data from the literature that are most likely to have grown in seawater of known composition. These

data include plankton tow samples with water collected concurrently, and sea-ice diatom samples filtered directly from melted pack ice (Varela et al., 2004; Cardinal et al., 2005; Fripiat et al., 2009; Fig. 6). We also include a core-top sample from a nutrient-rich region of coastal Antarctica (Table 1), where the seasonal uptake of Si(OH)_4 is relatively low such that the water is unlikely to experience large variations in $\delta^{30}\text{Si(OH)}_4$. The apparent fractionation is also known from culture experiments, and varies between -0.4 to -1.6‰, with an average value of -1.1‰ (de la Rocha et al., 1997). The compiled data suggest that diatoms carry out statistically significant greater apparent fractionation in higher Si(OH)_4 concentrations ($R^2 = 0.49$, $n = 27$). This apparent increase in fractionation factor with Si(OH)_4 concentration could be a result of uncertainty in the relationship between the water samples and the diatom samples (e.g. Cardinal et al., 2005). This finding would be consistent with culture experiments that appear to show that the fractionation factor in diatoms is approximately constant (de la Rocha et al., 1997). However, it is also possible that the link between Si(OH)_4 concentration and Si isotope fractionation by sponges is a real biological phenomenon and further investigation is required to prove or disprove such a relationship.

3.3. Core-top spicules

The core-top $\delta^{30}\text{Si}$ data for sponges, for samples located near seawater silicon isotope measurements or from well-characterized water masses, agree well with the calibration for living specimens (Fig. 2A, B). As with other studies of this nature, it is challenging to find co-located samples with a global distribution of the ideal range of

silicic acid concentrations. In this study, we have combined targeted collections with existing cores selected to be near existing water silicon isotope analyses. The one exception is the Si isotope composition of the Okhotsk Sea, which is not yet known, so the value used here is from the North East Pacific as reported in Beucher et al. (2008).

The agreement between core-top spicules and modern sponges indicate there is no significant influence of early post-depositional dissolution or diagenesis on sponge $\delta^{30}\text{Si}$. Laboratory studies carried out by Demarest et al (2009) on diatom cultures show that the impact of dissolution on diatom opal $\delta^{30}\text{Si}$ is measurable but unlikely to be significant in sediments, suggesting sponge and diatom opal may behave in a similar way in a post-depositional setting.

The core-top calibration shows less scatter than values based on measurements of individual modern sponges. This could be in part a consequence of the fact that there are fewer core-top measurements and in part that some of the core-top values were measured using Mg doping, whereas all of the modern sponges were measured by conventional standard-sample bracketing. However, the improvement in uncertainty afforded by Mg doping is less than the scatter in the modern calibration data and cannot explain all of the variability observed. This result suggests that there is some natural variability between individuals, possibly due to small-scale variation in Si(OH)_4 concentration or variable physiological conditions, which is averaged out through the mixing of spicules from different individuals during early sedimentation.

Although the relationship between $\delta^{30}\text{Si}$ and $\text{Si}(\text{OH})_4$ is non-linear (Fig. 2A), the proxy works well in a range (between 5-120 μM) suitable for the majority of Quaternary paleoceanographic applications. Taking the data within this range, it is possible to simplify the fractionation model described above by assuming a linear relationship between 5-120 μM , or by assuming a hyperbolic relationship between $\text{Si}(\text{OH})_4$ and $\delta^{30}\text{Si}$ ($R^2 = 0.95$, $n=8$, for samples $<120 \mu\text{M}$; $R^2 = 0.95$, $n=9$, for all samples) or $\Delta\delta^{30}\text{Si}$ ($R^2 = 0.99$, $n=8$, for samples $<120 \mu\text{M}$; $R^2 = 0.92$, $n=9$, for all samples). The function that best fits the relationship between $\text{Si}(\text{OH})_4$ and $\Delta\delta^{30}\text{Si}$ is given by Equation 8 (numbers in parentheses show $1\sigma_{\text{SD}}$):

$$\Delta\delta^{30}\text{Si} = -6.54 (0.60) + 270(20)/\{53(20) + \text{Si}(\text{OH})_4\} \quad (8)$$

Statistical analyses indicate that this fit can predict $\text{Si}(\text{OH})_4$ within $\pm 15 \mu\text{M}$, which is an improvement on previously reported uncertainty based on individual sponges (Fig. 7). Although it would be beneficial to obtain more data from other core-top locations to test the proxy further, our results from modern and core-top samples demonstrate that the $\delta^{30}\text{Si}$ value of sponge spicules from sediments can be used to reconstruct past $\text{Si}(\text{OH})_4$ concentrations in the ocean, and these analyses are well suited to addressing paleoceanographic questions relating to the cycling and transport of silica. Given the analytical uncertainties involved and the residence time of Si in the ocean, the relevant timescale and problems that can be addressed are on the order of $\sim 10 \text{ ka}$, over which whole ocean changes in $\delta^{30}\text{Si}$ are unlikely to impact biogenic opal isotopic compositions (Georg et al., 2009). For example, one of the key applications of the

* Note: $\Delta\delta^{30}\text{Si}$ and $\text{Si}(\text{OH})_4$ were mistakenly switched in published version

sponge $\delta^{30}\text{Si}$ proxy, tracing the movement of major water masses over glacial-interglacial timescales, requires only the distinction between high $\text{Si}(\text{OH})_4$ ($>100\ \mu\text{M}$) and low $\text{Si}(\text{OH})_4$ ($<30\ \mu\text{M}$) concentrations.

4. SUMMARY

In this study, we presented a calibration of modern individual sponge specimens and core-top spicules from different ocean basins. We show the relationship between sponge $\delta^{30}\text{Si}$ and $\text{Si}(\text{OH})_4$ is the same between different ocean basins and water masses with different temperature and salinity profiles. This result provides robust evidence that $\text{Si}(\text{OH})_4$ is indeed the major controlling factor in determining apparent sponge Si fractionation. The relationship between $\delta^{30}\text{Si}$ and $\text{Si}(\text{OH})_4$ is consistent with a fractionation model, where Si isotopes are fractionated by sponges during uptake, polymerization and efflux. We also show that core-top $\delta^{30}\text{Si}$ values agree well with the $\text{Si}(\text{OH})_4$ calibration of living sponges, indicating there are no significant post-depositional, dissolution or early diagenetic overprints, which have been found to impact other biogenic opal geochemical proxies.

Acknowledgements:

The authors would like to thank the following for collection of sponge specimens: Dann Blackwood (USGS, Woods Hole), Rhian Waller (University of Maine), Chris Kelley (University of Hawaii), Nicholas White (University of Cambridge), Jade Berman and Andy Clarke (British Antarctic Survey). Further specimens were obtained from the Smithsonian. Hawaiian samples were collected with Papahānaumokuākea Monument permit # PMNM-2009-053. Core samples were obtained with the assistance of Lloyd Keigwin and Ellen Roosen (WHOI), Stefan Mulitza (University of Bremen), Claire Allen and Claus-Deiter Hillenbrand (BAS), and Jerry McManus (Lamont Doherty Earth Observatory, Columbia University). Many thanks to Jurek Blusztjan and Maureen Auro (WHOI), Mark Brzezinski and Charlotte Beucher (University of California Santa Barbara), Ros Rickaby and Alex Halliday (Oxford University) for assistance in the laboratory, and with analyses and discussion. Thanks to Mark Brzezinski, Martin Wille,

James McManus and an anonymous reviewer for constructive reviews of the manuscript. Many thanks to the captain and crew of the R/V Nathaniel B Palmer (dredge samples were collected on cruises NBP0805 and NBP1103). This work was funded by the National Science Foundation (MGG grants 1029986; OPP ANT grants 0944474 and 0902957) and with the support of a WHOI Doherty Scholarship.

References:

- Anand, P. and Elderfield, H., 2005. Variability of Mg/Ca and Sr/Ca between and within the planktonic foraminifers *Globigerina bulloides* and *Globorotalia truncatulinoides*. *Geochemistry Geophysics Geosystems* **6**: doi:10.1029/2004GC000811.
- Barker, S., Greaves, M. et al., 2003. A study of cleaning procedures used for foraminiferal Mg/Ca paleothermometry. *Geochemistry Geophysics Geosystems* **4**, 8407.
- Beucher, C. P., Brzezinski, M. A., and Jones, J. L., 2008. Sources and biological fractionation of silicon isotopes in the Eastern Equatorial Pacific. *Geochimica et Cosmochimica Acta* **72**, 3063-3073.
- Brown, S. J. and Elderfield, H., 1996. Variations in Mg/Ca and Sr/Ca ratios of planktonic foraminifera caused by postdepositional dissolution: evidence of a shallow Mg-dependent dissolution. *Paleoceanography* **11**, 543-551.
- Nelson, D.K., Brzezinski, M.A., Sigman, D.E., and Franck, V.M., 2001, A seasonal progression of Si limitation in the Pacific sector of the Southern Ocean. *Deep-Sea Research II*, **48**, 3973-3995.
- Brzezinski, M. A., Sigman, D. M., Sarmiento, J. L., Matsumoto, K., Gruber, N., Rau, G. H., and Coale, K. H., 2002. A switch from Si(OH)_4 to NO_3^- depletion in the glacial

506 Southern Ocean. *Geophysical Research Letters* **29**, 1564.

507 Cardinal, D., Alleman, L. Y., de Jong, J., Ziegler, K., and Andre, L., 2003. Isotopic
508 composition of silicon measured by multicollector plasma source mass
509 spectrometry in dry plasma mode. *Journal of Analytical Atomic Spectrometry* **18**,
510 213-218.

511 Cardinal, D., Alleman, L. Y., Dehairs, F., Savoye, N., Trull, T. W., and Andre, L., 2005.
512 Relevance of silicon isotopes to Si-nutrient utilization and Si-source assessment
513 in Antarctic waters. *Global Biogeochemical Cycles* **19**,
514 doi:10.1029/2004GB002364.

515 Cardinal, D., Savoye, N., Trull, T. W., Dehairs, F., E.E., K., Fripiat, F., Tison, J.-L., and
516 André, L., 2007. Silicon isotope in spring Southern Ocean diatoms: large zonal
517 changes despite homogeneity among size fractions. *Marine Chemistry* **106**, 46-
518 62.

519 de la Rocha, C., Brzezinski, M. A., and DeNiro, M. J., 1997. Fractionation of silicon
520 isotopes by marine diatoms during biogenic silica formation. *Geochimica*
521 *Cosmochimica Acta* **61**, 5051-5056.

522 de la Rocha, C., Brzezinski, M. A., DeNiro, M. J., and Shemesh, A., 1998. Silicon isotope
523 composition of diatoms as an indicator of past oceanic change. *Nature* **395**, 680-
524 683.

525 de la Rocha, C. L., Brzezinski, M. A., and DeNiro, M. J., 2000. A first look at the
526 distribution of the stable isotopes of silicon in natural waters. *Geochimica et*
527 *Cosmochimica Acta* **64**, 2467-2477.

528 de la Rocha, C. and Bickle, M., 2005. Sensitivity of silicon isotopes to whole-ocean

529 changes in the silica cycle. *Marine Geology* **217**, 267-282.

530 Demarest, M. S., Brzezinski, M. A., and Beucher, C., 2009. Fractionation of silicon
531 isotopes during biogenic silica dissolution. *Geochimica et Cosmochimica Acta* **73**,
532 5572-5583.

533 Dixit, S. and Van Cappellen, P., 2002. Surface chemistry and reactivity of biogenic silica.
534 *Geochimica Cosmochimica Acta* **66**, 2559-2568.

535 Elderfield, H. and Ganssen, G., 2000. Past temperature and $\delta^{18}\text{O}$ of surface ocean waters
536 inferred from foraminiferal Mg/Ca ratios. *Nature* **405**, 442-445.

537 Elderfield, H., Vautravers, M. et al., 2002. The relationship between shell size and
538 Mg/Ca, Sr/Ca, $\delta^{18}\text{O}$, and $\delta^{13}\text{C}$ of species of planktonic foraminifera.
539 *Geochemistry Geophysics Geosystems* **3**, doi:10.1029/2001GC000194.

540 Ellwood, M. J., Wille, M., and Maher, W., 2010. Glacial silicic acid concentrations in the
541 Southern Ocean. *Science* **330**, 1088-1091.

542 Falkowski, P. G., Katz, M. E., Knoll, A. H., Quigg, A., Raven, J. A., Schofield, O., and Taylor,
543 F. J. R., 2004. The evolution of modern eukaryotic phytoplankton. *Science* **305**,
544 354-360.

545 Ferguson, J. E., G. M. Henderson, et al., 2008. Systematic change of foraminiferal Mg/Ca
546 ratios across a strong salinity gradient. *Earth and Planetary Science Letters* **265**,
547 153-166.

548 Fripiat, F., Cardinal, D., Tison, J.-L., Worby, A., and André, L., 2007, Diatom-induced
549 silicon isotopic fractionation in Antarctic sea ice. *Journal of Geophysical*
550 *Research*, **112**, doi:10.1029/2006JG000244.

551 Frøhlich, H. and Barthel, D., 1997. Silica uptake of the marine sponge *Halichondria*

552 *panicea* in Kiel Bight. *Marine Biology* **128**, 115-125.

553 Galy, A., Belshaw, N. S., Halicz, L., and O'Nions, R. K., 2001. High-precision measurement
 554 of magnesium isotopes by multiple-collector inductively coupled plasma mass
 555 spectrometry. *International Journal of Mass Spectrometry* **208**, 89-98.

556 Georg, R. B., Reynolds, B. C., Frank, M., and Halliday, A. N., 2006. New sample
 557 preparation techniques for the determination of Si isotopic composition using
 558 MC-ICPMS. *Chemical Geology* **235**, 95-104.

559 Georg, R. B., West, A. J., Basu, A. R., and Halliday, A. N., 2009. Silicon fluxes and isotope
 560 composition of direct groundwater discharge into the Bay of Bengal and the
 561 effect on the global ocean silicon budget. *Earth and Planetary Science Letters*
 562 **283**, 67-74.

563 Hendry, K. R., Georg, R. B., Rickaby, R. E. M., Robinson, L. F., and Halliday, A. N., 2010a.
 564 Deep ocean nutrients during the Last Glacial Maximum deduced from sponge
 565 silicon isotopic compositions. *Earth and Planetary Science Letters* **292**, 290-300.

566 Hendry, K. R., Meredith, M. P., Measures, C. I., Carson, D. S., and Rickaby, R. E. M., 2010b.
 567 The role of sea ice formation in cycling of aluminium in northern Marguerite
 568 Bay, Antarctica. *Estuarine, Coastal and Shelf Science* **87**, 103-112.

569 Hendry, K.R., Leng, M.J., Robinson, L.F., Sloane, H.J., Blusztjan, J., Rickaby, R.E.M., Georg,
 570 R.B. & Halliday, A.N., 2011. Silicon isotopes in Antarctic sponges: an
 571 interlaboratory comparison. *Antarctic Science* doi:
 572 10.1017/S0954102010000593

573 Hendry, K.R., Robinson, L.F., Meredith, M.P., Mulitza, S., Cheissi, C., & Arz, H., in review.
 574 Abrupt changes in high-latitude nutrient supply to the Atlantic during the last
 575 glacial cycle.
 576 Jacques, G., 1983. Some ecophysiological aspects of Antarctic phytoplankton. *Polar*
 577 *Biology* **2**, 27-33.
 578 Keigwin, L. D., 1998. Glacial-age hydrography of the far northwest Pacific Ocean.
 579 *Paleoceanography* **13**, 323-339.
 580 Keigwin, L. D., 2001. Data report: Late Pleistocene stable isotope studies of ODP sites
 581 1054, 1055, and 1063. *Proceedings of the Ocean Drilling Program, Initial Reports.*
 582 *College Station, Texas (Ocean Drilling Program)* **172**, 1-14.
 583 Maldonado, M., Carmona, M. C., Uriz, M. J., and Cruzado, A., 1999. Decline in Mesozoic
 584 reef-building sponges explained by silicon limitation. *Nature* **401**, 785-788.
 585 Maldonado, M., Carmona, M.C., Velasquez, Z., Puig, A., Cruzado, A., Lopez, A., and Young,
 586 C.M., 2005, Siliceous sponges as a silicon sink: an overlooked aspect of
 587 benthopelagic coupling in the marine silicon cycle. *Limnology and*
 588 *Oceanography*, **50**, 799-809.
 589 Maldonado, M., and Riesgo, A., 2007, Intra-epitheial spicules in a homosclerophorid
 590 sponge: *Cell and Tissue Research*, **328**, 639-650.
 591 Maldonado, M., Navarro, L., Grasa, A., Gonzalez, A., and Vaquerizo, I., 2011. Silicon
 592 uptake by sponges: a twist to understanding nutrient cycling on continental
 593 margins. *Nature Scientific Reports* **1**, doi:10.1038/srep00030.
 594 Milligan, A. J., Varela, D. E., Brzezinski, M. A., and Morel, F. M. M., 2004. Dynamics of
 595 silicon metabolism and silicon isotopic discrimination in a marine diatom as a

596 function of pCO₂. *Limnology and Oceanography* 49, 322-329.

597 Müller, W.E.G., Li, J., Schroeder, H.C., Qiao, L., and Wang, X., 2007, The unique skeleton of
 598 siliceous sponges (Porifera; Hexactinellida and Demospongiae) that evolved
 599 first from the Urmetazoa during the Proterozoic: a review: *Biogeosciences*, **4**,
 600 219-232.

601 Paasche, E., 1973. Silicon and the ecology of marine plankton diatoms. II. Silicate-
 602 uptake kinetics in five diatom species. *Marine Biology* **19**, 262-269.

603 Reincke, T. and Barthel, D., 1997. Silica uptake kinetics of *Halichondria panicea* in Kiel
 604 Bight. *Marine Biology* **129**, 591-593.

605 Reynolds, B. C., 2009. Modeling the modern marine $\delta^{30}\text{Si}$ distribution. *Global*
 606 *Biogeochemical Cycles* **23**, GB2015, doi:10.1029/2008GB003266.

607 Reynolds, B. C., Aggarwal, J., Andre, L., Baxter, D., Beucher, C., Brzezinski, M. A.,
 608 Engstrom, E., Georg, R. B., Land, M., Leng, M. J., Opfergelt, S., Rodushkin, I.,
 609 Sloane, H. J., van der Boorn, S. H. J. M., Vroon, P. Z., and Cardinal, D., 2007. An
 610 inter-laboratory comparison of Si isotope reference materials. *Journal of*
 611 *Analytical Atomic Spectrometry* **22**, 561-568.

612 Sarmiento, J. L., Gruber, N., Brzezinski, M. A., and Dunne, J. P., 2004. High-latitude
 613 controls of thermocline nutrients and low latitude biological productivity.
 614 *Nature* **427**, 56-60.

615 Schröder, H. C., Wang, X. et al., 2008. Biofabrication of biosilica-glass by living
 616 organisms. *Natural Products Reports* **25**, 433-636.

617 Tréguer, P., Nelson, D. M., Van Bennekom, A. J., DeMaster, D. J., Leynaert, A., and
 618 Quéguiner, B., 1995. The silica balance in the world ocean: a reestimate. *Science* **268**,

619 375-379.

620 West, A. J., Galy, A., and Bickle, M., 2005. Tectonic and climatic controls on silicate
621 weathering. *Earth and Planetary Science Letters* **235**, 211-228.

622 Wille, M., Sutton, J., Ellwood, M. J., Sambridge, M., Maher, W., Eggins, S., and Kelly, M.,
623 2010. Silicon isotopic fractionation in marine sponges: a new model for
624 understanding silicon isotopic fractionation in sponges. *Earth and Planetary
625 Science Letters*, doi:10.1016/j.epsl.2010.01.036.

626 Wit, J. C., Reichart, G.-J., et al., 2010. Approaches to unravel seasonality in sea surface
627 temperatures using paired single-specimen foraminiferal $\delta^{18}\text{O}$ and Mg/Ca
628 analyses. *Paleoceanography* **25**, doi:10.1029/2009PA001857.

629 Van Beusekom, J. E. E., Bennekom, A. J., Tréguer, P., and Morvan, J., 1997. Aluminium
630 and silicic acid in water and sediments of the Enderby and Crozet Basins. *Deep-
631 Sea Research II* **44**, 987-1003.

632 Varela, D.E., Pride, C.J., and Brzezinski, M.A., 2004, Biological fractionation of silicon
633 isotopes in Southern Ocean surface waters. *Global Biogeochemical Cycles*, **18**,
634 doi:10.1029/2003GB002140.

635 Young, E. D., Galy, A., and Nagahara, H., 2002. Kinetic and equilibrium mass-dependent
636 isotope fractionation laws in nature and their geochemical and cosmochemical
637 significance. *Geochimica et Cosmochimica Acta* **66**, 1095-1104.

638

Figure 1: Location of samples in this study. The white circles show core-top samples, the black circles show living specimens (from this study, Hendry et al., 2010a and Wille et al., 2010). Drawn using GeoMapApp.

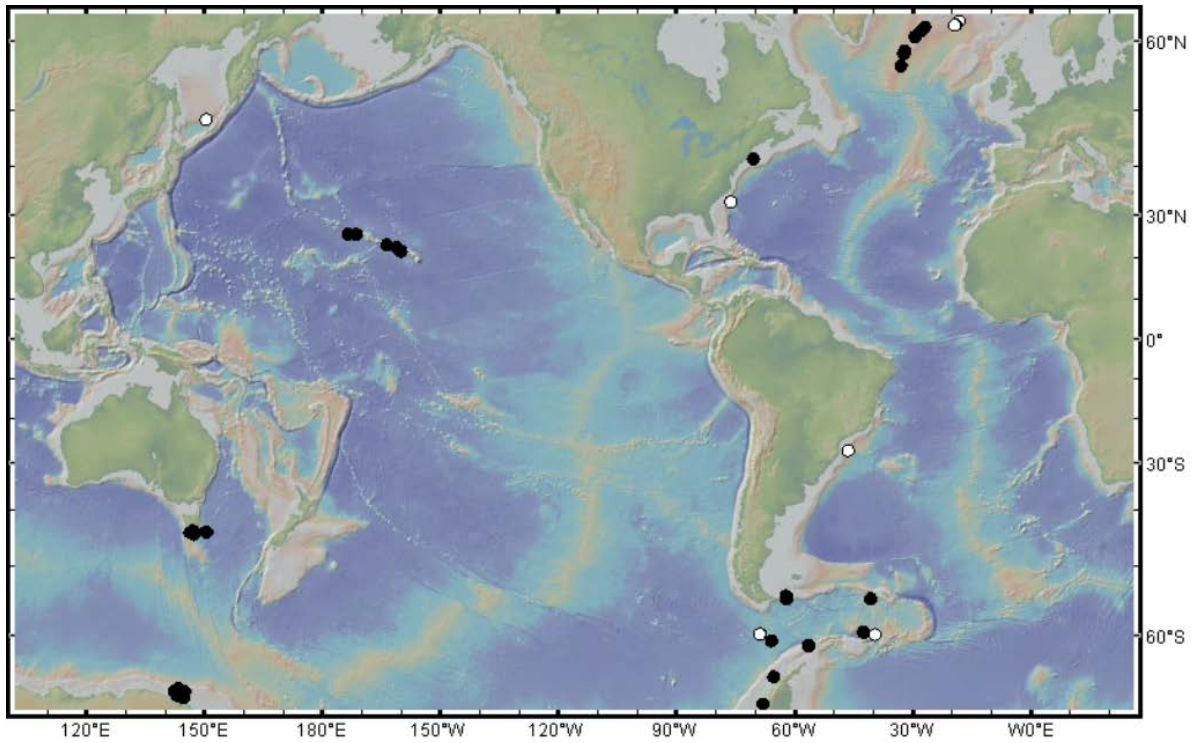


Figure 2: A) $\delta^{30}\text{Si}$ and B) $\Delta\delta^{30}\text{Si}$ for all sponges from different ocean basins. The modern sponges (open symbols) were measured without Mg doping, with error bars showing $2\sigma_{\text{SD}}$ ($\sim\pm 0.2\text{‰}$ for $\delta^{30}\text{Si}$ and 0.4‰ for $\Delta\delta^{30}\text{Si}$). The core-top spicules (solid symbols) were measured with Mg doping, with error bars showing $2\sigma_{\text{SD}}$ ($\sim\pm 0.1\text{‰}$ for $\delta^{30}\text{Si}$).

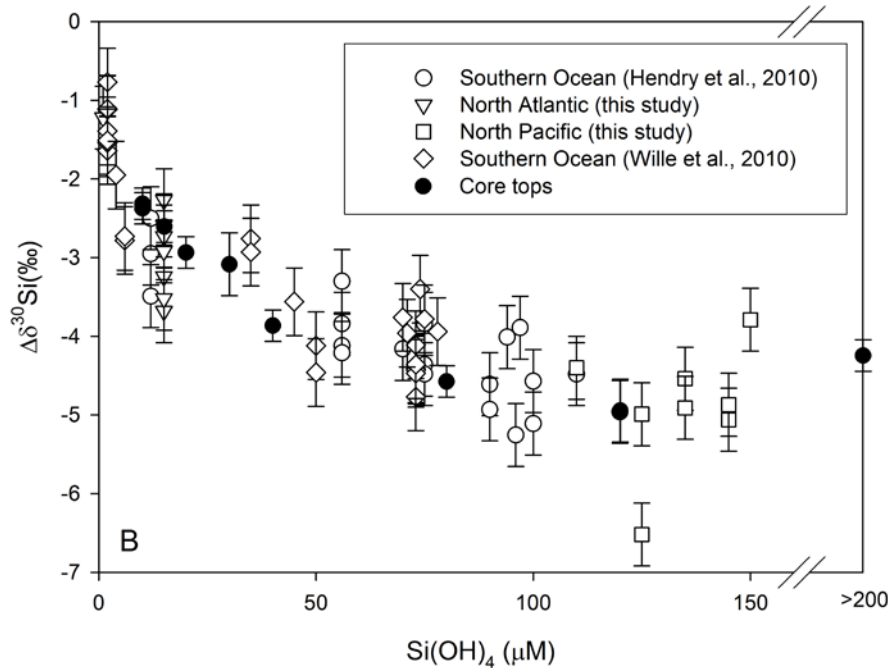
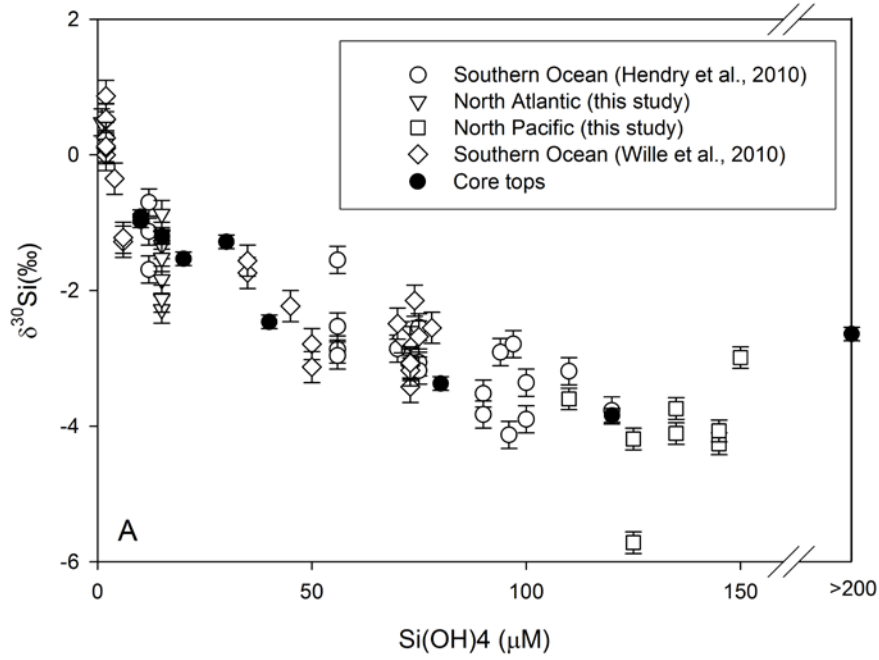


Figure 3: $\Delta\delta^{30}\text{Si}$ for all sponges from different ocean basins plotted against temperature (data from Hendry et al., 2010a; Wille et al., 2010; this study, www.ewoce.org, <http://www.nodc.noaa.gov>). Note that the larger number of samples from the Southern Ocean biases the relationship between apparent fractionation and temperature (grey symbols): the North Pacific and Atlantic data cover the same range of apparent fractionation values, but in a limited temperature window (black symbols). $2\sigma_{\text{SD}}$ on $\Delta\delta^{30}\text{Si}$ values $\sim 0.4\text{‰}$.

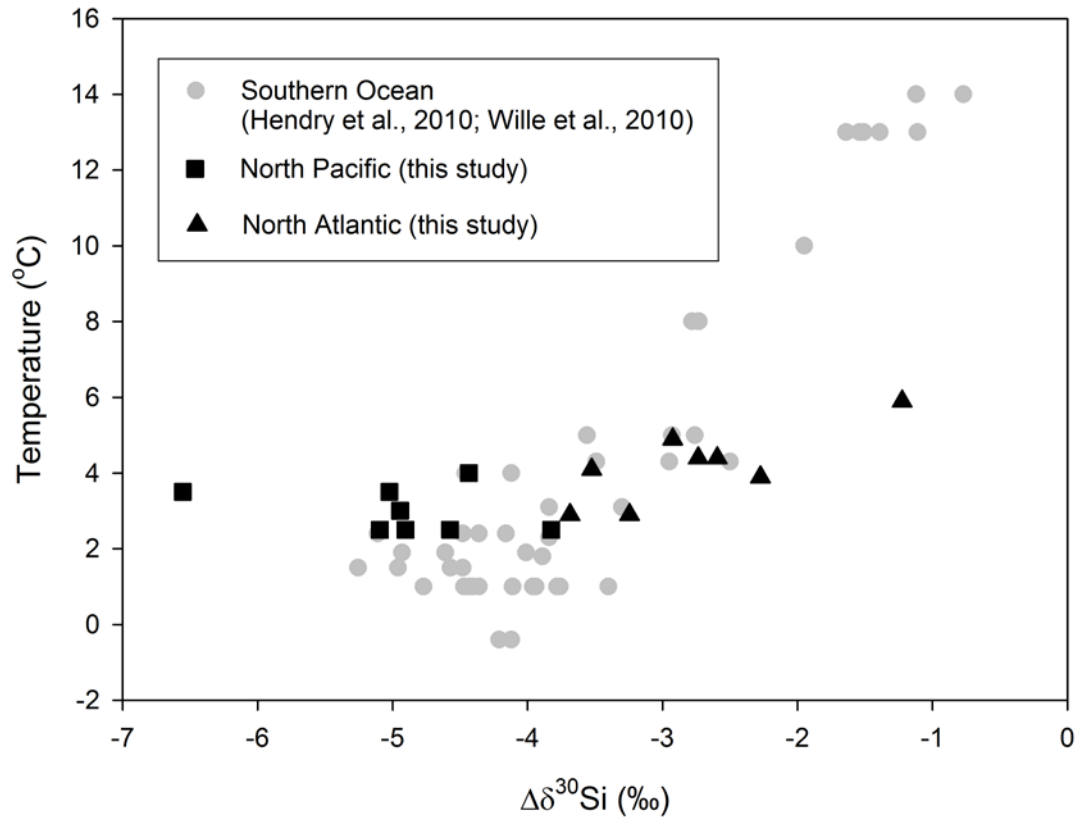
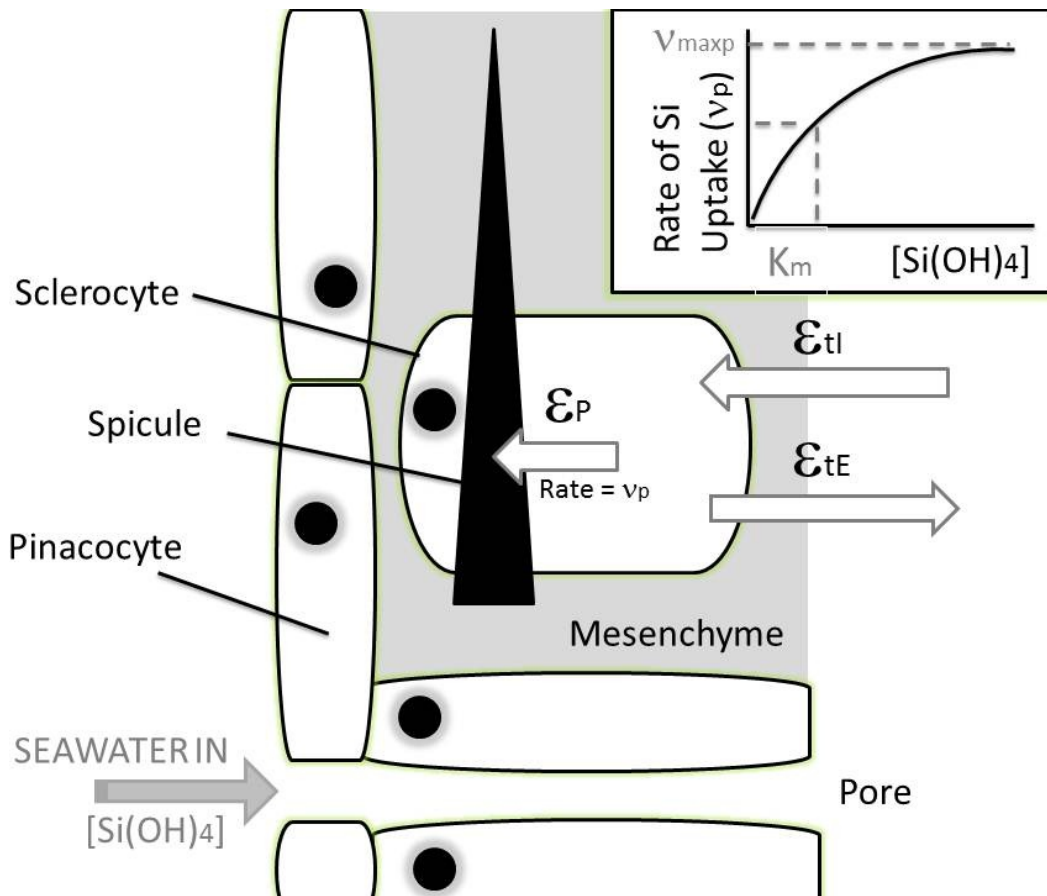
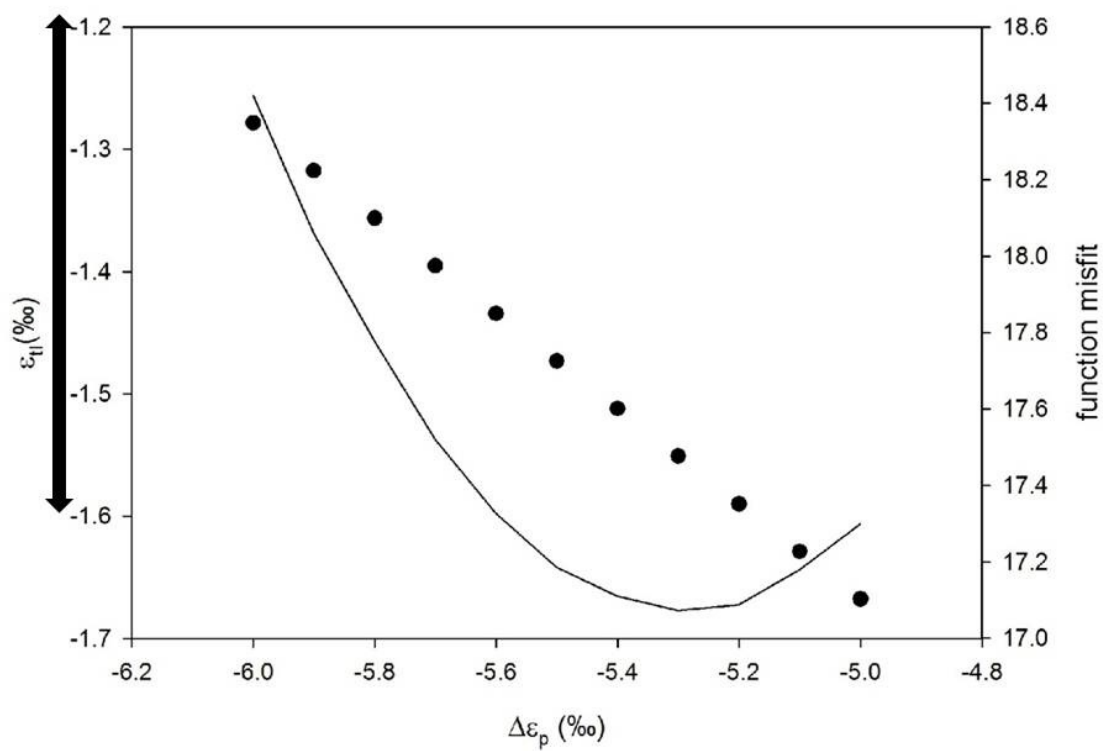
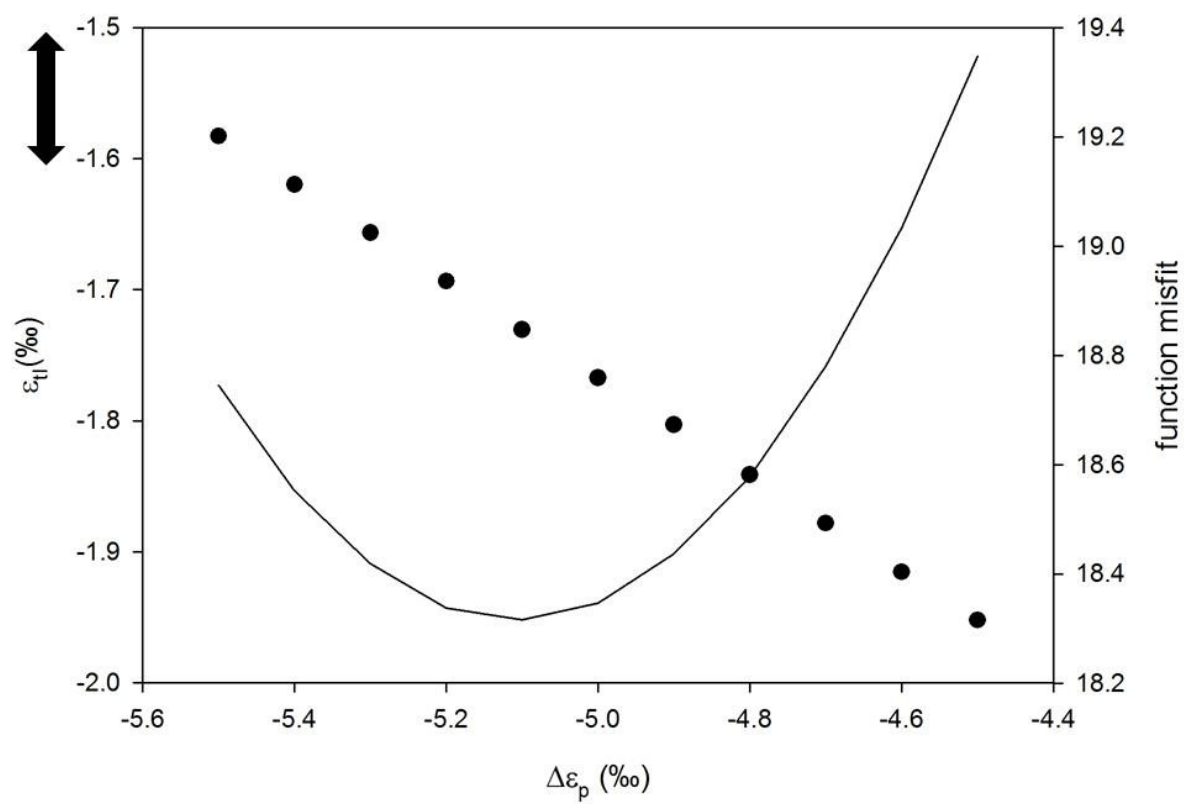


Figure 4: Fractionation of Si isotopes by sponges during uptake processes. A) A cartoon of the fractionation model used in this study. It should be noted that the model used here is a simplification of sponge silicification, and other models for silicification mechanisms exist (e.g. Müller et al., 2007; Maldonado & Riesgom 2007). Seawater enters the sponge via pores, lined with pinacocyte cells, and is taken up into the sclerocyte cells where silica formation is initiated. Silicification of large spicules occurs extracellularly in association with an organic matrix, and is controlled by protein interactions (Schröder et al., 2008). The fractionation parameters are described in the main text. B-C) The misfit between predicted ϵ_f and observed $\Delta\delta^{30}\text{Si}$ for the whole dataset (the misfit function is defined as $(\epsilon_f - \Delta\delta^{30}\text{Si})^2$ shown by the solid line), and corresponding value of ϵ_{tl} that results in the minimum misfit (circles), for different values of $\Delta\epsilon_p$ substituted into Equations 4 and 5, using values from B) Reincke & Barthel, 1997 and C) Maldonado et al., 2011. The isotope data for sponges grown in low $\text{Si}(\text{OH})_4$ conditions ($<2 \mu\text{M}$) show an average $\Delta\delta^{30}\text{Si}$ of $-1.3 \pm 0.3\text{‰}$ (σ_{SD}), shown by the black arrows, which should equal the value of ϵ_{tl} .





676



677

678

Figure 5: The observed $\Delta\delta^{30}\text{Si}$ vs. ε_f predicted using the sponge silicon uptake model for the uptake kinetics of Reincke & Barthel, 1997 and Maldonado et al., 2011 (shown as inset). The solid lines show the 1:1 slope $\pm 2\sigma_{\text{SD}}$ uncertainty for the $\Delta\delta^{30}\text{Si}$ values. Error bars show $\pm 2\sigma_{\text{SD}}$.

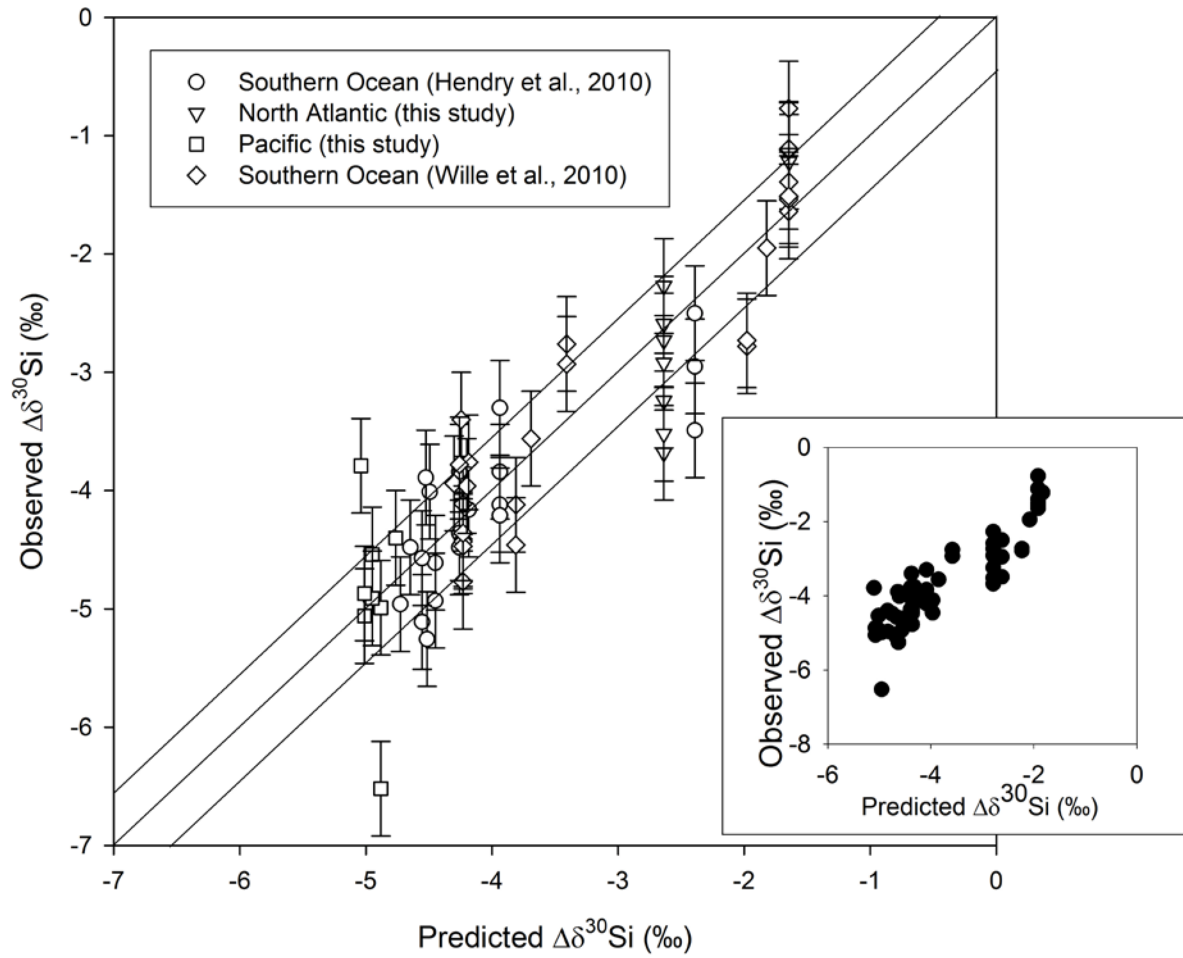
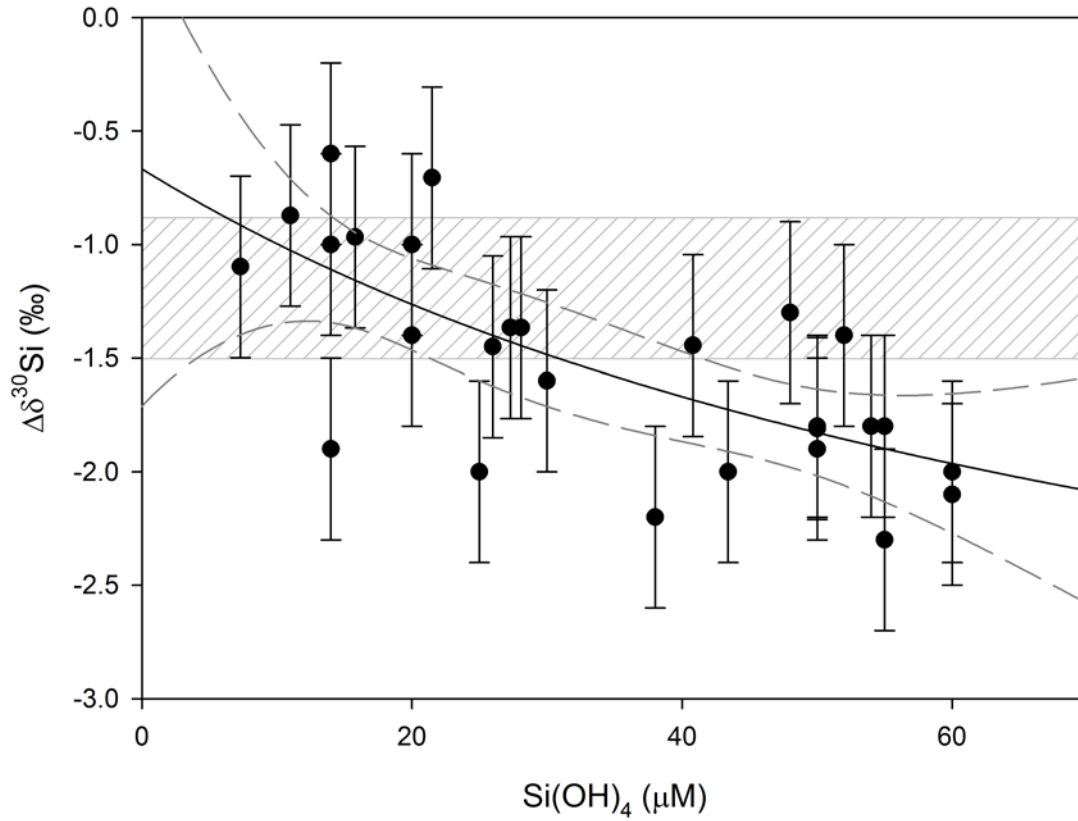
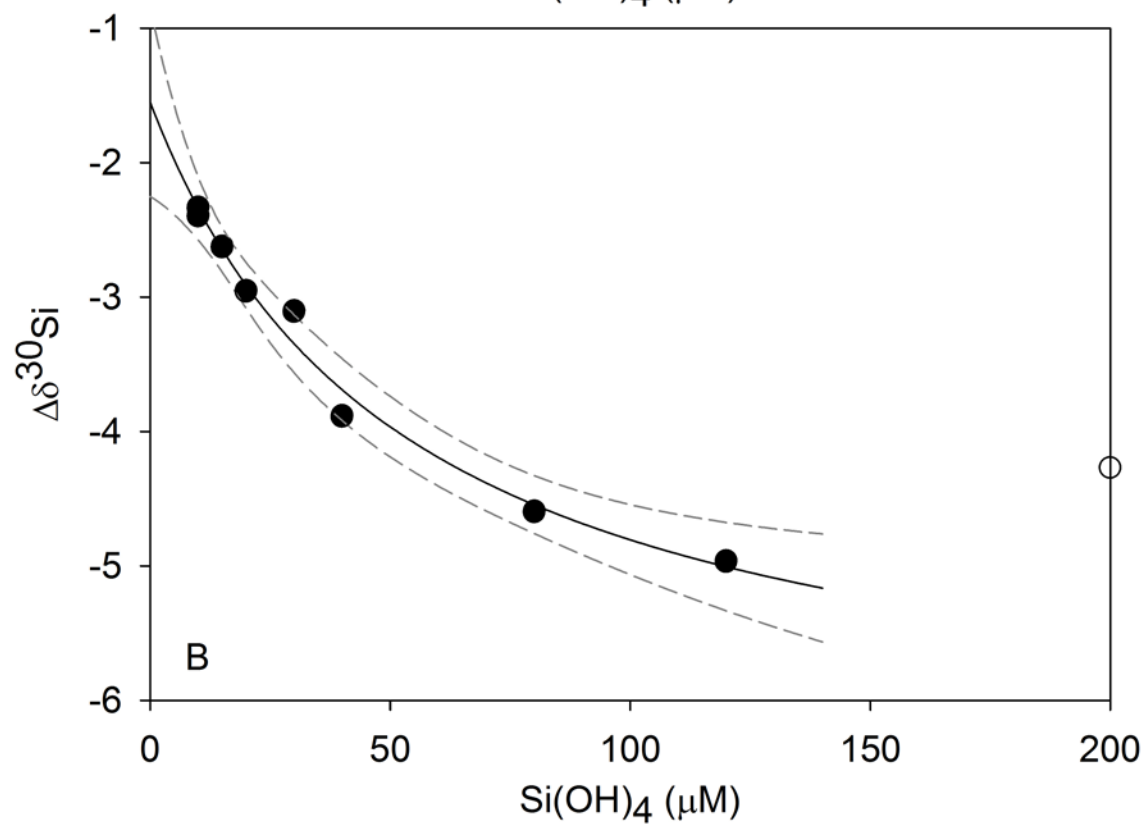
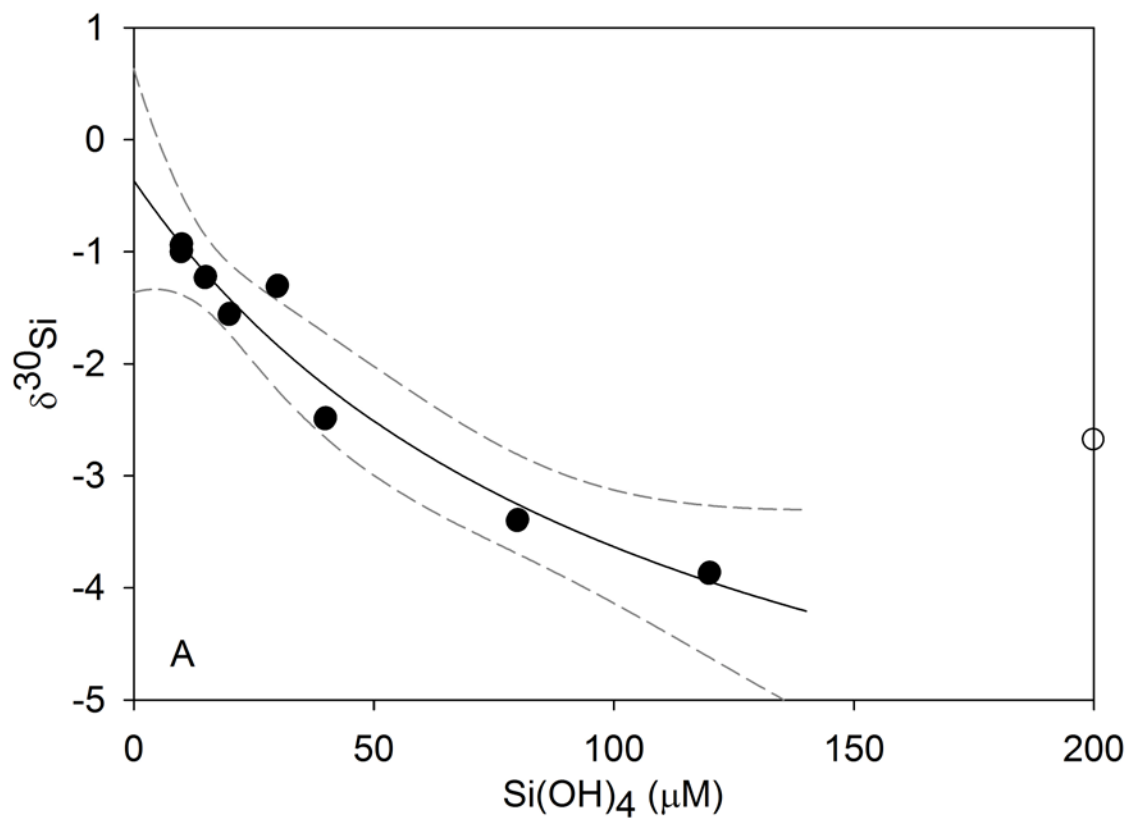


Figure 6: Field data showing the apparent change in diatom fractionation factor with ambient Si(OH)_4 concentration. Data from Varela et al., 2004; Cardinal et al., 2005, Fripiat et al., 2009, and the core-top diatom value from Table 1 ($2\sigma_{\text{SD}}$ on $\Delta\delta^{30}\text{Si}$ values $\sim 0.4\text{‰}$). The grey bar shows the fractionation factor of -1.1‰ from de la Rocha et al., 1997, with the same uncertainty of $\pm 0.4\text{‰}$. The dashed lines show the 95% confidence level.



693 Figure 7: Core-top calibration of A) $\delta^{30}\text{Si}$ and B $\Delta\delta^{30}\text{Si}$ of sponges versus $\text{Si}(\text{OH})_4$. The
694 solid line shows the predicted $\text{Si}(\text{OH})_4$ using the regression analysis and the dashed
695 lines show the 95% confidence interval. The solid symbols show the samples used in
696 the regression analysis ($<120\text{ mM}$) and the open symbol shows the sample from the
697 Okhotsk Sea).



699

700

701

Specimen	Species	Lat	Long	Depth (m)	Si(OH) ₄ (μM)	δ ²⁹ Si (‰)	δ ³⁰ Si (‰)
<i>LMG08</i> ^a	Unknown	64.78 S	68.23 W	600	105- 110	-1.75 (0.06)	-3.43 (0.15)
<i>LMG08</i> ^b						-1.77 (0.04)	-3.44 (0.09)
<i>LMG08</i> ^c						-1.72 (0.07)	-3.37 (0.17)
<i>LMG08</i> ^d							-3.33
<i>N. Atlantic</i>							
D10 ^a	Unknown	56.88 N	33.00 W	2150	15	-0.89	-1.84
D18 ^e	Unknown	58.51 N	32.32 W	1520	15	-0.45	-0.87
D19A ^e	Unknown	58.90 N	31.98 W	1720	15	-1.12	-2.28
D26 ^a	Unknown	60.72 N	29.45 W	1250	15	-1.00	-2.12
D29 ^a	Unknown	61.41 N	27.86 W	1105	15	-0.61	-1.19
D30A ^a	Unknown	61.57 N	27.56 W	1021	15	-0.73	-1.33
D31A ^a	Unknown	61.87 N	27.01 W	864	15	-0.75	-1.52
Woods Hole ^a	Unknown	41.53 N	70.67 W	10	<1	+0.21	+0.48
<i>Pacific</i>							
P4-299-10 ^a	Unknown	22.72 N	161.67 W	1000	110	-1.87	-3.60
1097479 ^a	<i>Caulophacus</i>	25.80 N	173.43 W	1798	145	-2.05	-4.07
1097480 ^a	sp.	25.80 N	173.43 W	1802	145	-2.19	-4.27
1097533 ^a	Hexactinellid	25.70 N	171.45 W	1810	150	-1.52	-2.92
	<i>Farrea</i> sp.					-1.56	-3.06
1097536 ^a		25.70 N	171.45 W	1488	135	-2.12	-4.11
1097539 ^a	Hexactinellid	25.67 N	171.41 W	1206	125	-2.99	-5.72
1097541 ^a	<i>Farrea</i> sp.	25.67 N	171.41 W	1206	125	-2.13	-4.19
1097570 ^a	<i>Bathydorus</i> sp.	23.30 N	163.68 W	1443	135	-1.91	-3.74
	<i>Trichasterina</i>						
<i>Dredge sediments</i>	sp.						

Sars sea-mount NBP0805- DR34 ^a		59.73 S	68.73 W	850	80	-1.77	-3.39
NBP1103- DH91 ^a		59.72 S	68.87 W	650	40	-1.30	-2.59
NBP1103- DH91 ^b						-1.29	-2.48
<i>Core-top spicules</i>							
Newmeyanov, 25, GGC15 ^a		51.1 N	168.1 W	1980	200	-1.32	-2.66
Newmeyanov, 25, GGC15 ^b						-1.26	-2.53
KNR-140-2- GGC56 ^a		32.94 N	76.30 W	1400	15	-0.66	-1.27
KNR-140-2- GGC56 ^b						-0.60	-1.22
ATII-94-1PC ^b		62.58 N	18.23 W	1177	10	-0.46	-0.99
ATII-94-9PG ^a		62.12 N	19.04 W	2090	20	-0.83	-1.61
ATII-94-9PG ^b						-0.72	-1.55
ATII-94-10PC ^b		62.15 N	19.33 W	1564	10	-0.40	-0.93
GeoB2107 ^a		27.18 S	46.45 W	1048	30	-0.68	-1.27
PC034 ^e		59.79 S	39.60 W	1652	120	-1.96	-3.86
Diatom samples from Ryder Bay, Antarctica (core BC388) ^e		67.57 S	68.23 W	500	60	-0.03	-0.01

702	a =measured by Neptune MC-IC-MS (WHOI) without Mg doping (typically mean of triplicate						
703	measurements); b = measured by Neptune MC-IC-MS (WHOI) with Mg doping; c = mean value from 3						
704	different laboratories from Hendry et al., 2010b; d = measured by M. Brzezinski and C. Beucher (UCSB)						
705	by IRMS, shown as the mean of two duplicates; e = measured by NuPlasma MC-ICP-MS (Oxford) without						
706	Mg doping (Hendry et al., 2010a). Numbers in parentheses show $2\sigma_{SD}$ long-term variability. Silicic acid						
707	concentrations are estimated from ewoce sections (www.ewoce.org) with an approximate error of $5\mu\text{M}$,						
708	which has not been taken into consideration in the statistical analysis.						
709	Table 1: Samples and silicon isotopic compositions of modern sponges and core-tops.						
710							

711 Table 2: Seawater $\delta^{30}\text{Si}(\text{OH})_4$ values used in this study; ^a from de la Rocha et al. (2000);
712 ^b from Hendry et al. (2010a); ^c from Wille et al. (2010) adapted from Cardinal et al.
713 (2005); ^d from Beucher et al. (2008).

Ocean basin/water mass	Depth (m)	$\delta^{30}\text{Si}(\text{OH})_4$ (‰)
North Atlantic	1000-2000	+1.4 ^a
North Pacific	1000-2000	+0.8 ^a
Southern Ocean		
AAIW	~300	+1.8 ^b
CDW	400-1000	+1.3 to +1.4 ^{b,c}
	1000-2000	+1.1 ^{b,c}
Sub-surface (depleted $\text{Si}(\text{OH})_4$)	50-150	+1.7 to +1.9 ^{a,c,d}
North Pacific (highly enriched in $\text{Si}(\text{OH})_4$)	2000-2500	+1.6 to +1.7 ^d
Near surface in Ryder Bay, Antarctica		+1.8 ^b

714

715